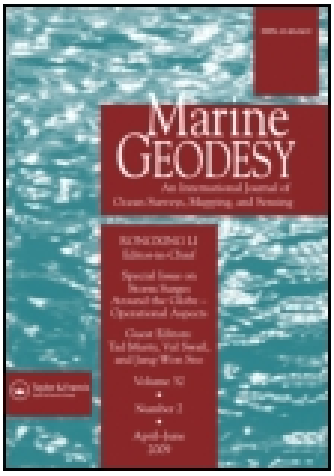


Marine Geodesy
Publication details, including instructions for authors and subscription information:
http://www.tandfonline.com/loi/umgd20

# Satellite Remote Sensing as a Reconnaissance Tool for Assessing Nautical Chart Adequacy and Completeness

Shachak Pe'eri[a], Christopher Parrish[b], Chukwuma Azuike[ac], Lee Alexander[a] & Andrew Armstrong[b]

[a] Center for Coastal and Ocean Mapping, University of New Hampshire, Durham, NH, USA

[b] National Oceanic and Atmospheric Administration, Silver Spring, MD, USA

[c] Nigerian Navy Hydrographic Office, Lagos, Nigeria

Accepted author version posted online: 21 Apr 2014.Published online: 19 Jun 2014.

To cite this article: Shachak Pe'eri, Christopher Parrish, Chukwuma Azuike, Lee Alexander & Andrew Armstrong (2014) Satellite Remote Sensing as a Reconnaissance Tool for Assessing Nautical Chart Adequacy and Completeness, Marine Geodesy, 37:3, 293-314, DOI: 10.1080/01490419.2014.902880

To link to this article: http://dx.doi.org/10.1080/01490419.2014.902880

*Marine Geodesy*, 37:293–314, 2014

ISSN: 0149-0419 print / 1521-060X online
DOI: 10.1080/01490419.2014.902880

Taylor & Francis
Taylor & Francis Group

# Satellite Remote Sensing as a Reconnaissance Tool for Assessing Nautical Chart Adequacy and Completeness

SHACHAK PE'ERI,[1] CHRISTOPHER PARRISH,[2] CHUKWUMA AZUIKE,[1,3] LEE ALEXANDER,[1] AND ANDREW ARMSTRONG[2]

[1]Center for Coastal and Ocean Mapping, University of New Hampshire, Durham, NH, USA
[2]National Oceanic and Atmospheric Administration, Silver Spring, MD, USA
[3]Nigerian Navy Hydrographic Office, Lagos, Nigeria



*National hydrographic offices need a better means of assessing the adequacy of existing nautical charts in order to plan and prioritize future hydrographic surveys. The ability to derive bathymetry from multispectral satellite imagery is a topic that has received considerable attention in scientific literature. However, published studies have not addressed the ability of satellite-derived bathymetry to meet specific hydrographic survey requirements. Specifically, the bathymetry needs to be referenced to a chart datum and statistical uncertainty estimates of the bathymetry should be provided. Ideally, the procedure should be based on readily-available, low-cost software, tools, and data. This paper describes the development and testing of a procedure using publicly-available, multispectral satellite imagery to map and portray shallow-water bathymetry in a GIS environment for three study sites: Northeast United States, Nigeria, and Belize. Landsat imagery and published algorithms were used to derive estimates of the bathymetry in shallow waters, and uncertainty of the satellite-derived bathymetry was then assessed using a Monte Carlo method. Results indicate that the practical procedures developed in this study are suitable for use by national hydrographic offices.*

**Keywords** Bathymetry, nautical charting, remote sensing, satellite imagery, water clarity, Landsat

## Introduction

National hydrographic offices need to periodically assess the adequacy of information on existing nautical charts for survey planning and prioritization (Azuike et al. 2012). The goal of such an assessment is not to directly produce chart updates but rather to obtain quantifiable information related to the amount of change since the last hydrographic survey upon which the charted information is based. When charting resources are limited,

Received 28 January 2013; accepted 17 February 2014.
Address correspondence to Shachak Pe'eri, Assistant Research Professor, Center for Coastal and Ocean Mapping, 24 Colovos Road, Durham, NH 03824. E-mail: shachak@ccom.unh.edu
Color versions of one or more of the figures in the article can be found online at www.tandfonline.com/umgd.

particularly in developing nations, these assessments provide beneficial information to optimize the use of available resources. One of the key factors related to the suitability of a nautical chart is the adequacy of the charted bathymetry. Hence, there is a need for low-cost, up-to-date reconnaissance surveys with known accuracies and uncertainties for bathymetric information. Good estimates of the uncertainty of the bathymetry are critical, even if the data do not meet International Hydrographic Organization (IHO) S-44 survey standards (Su et al. 2008). Hydrographic surveying offices increasingly expect all data to be accompanied by statistical estimates of uncertainty, as specified by IHO. Also, these uncertainties enable the hydrographic survey offices to evaluate the suitability of the data for applications beyond direct application of soundings to the chart, such as coastal change analysis and coastal zone management.

Satellite-derived bathymetry from multispectral remote sensing provides a cost-effective tool for chart adequacy assessment. Bathymetry derived from multispectral imagery has received significant attention in published literature in recent decades (e.g., Lyzenga 1978; Lyzenga et al. 1985; Philpot 1989; Stumpf et al. 2003; Louchard et al. 2003; Lyzenga 2006; Vanderstraete et al. 2006; Hogfe et al. 2008; Su et al. 2008; Bachmann et al. 2012; Flener et al. 2012; Bramante et al. 2013). Previous studies have primarily focused on the development of new algorithms. Although these studies are useful, they have not answered a fundamental question: Can hydrographic offices use these algorithms to derive bathymetry for charting evaluation?

The goal of this study is to develop and test a satellite-derived bathymetry procedure suitable for use by hydrographic offices. The procedure is based on algorithms from previous studies and operates on commercial-off-the-shelf (COTS) Geographic Information Systems (GIS) software. Key criteria for success of the satellite-derived bathymetry procedure are: 1) to provide an approach to reference the bathymetry to chart datum (typically a tidal datum, such as Mean Lower Low Water), and 2) to assess the total propagated uncertainty (TPU) of the derived bathymetry using statistical analysis. The procedure is based on data, tools, and algorithms that are readily available to hydrographic offices in developing nations and will be amenable to transitioning from research to operations.

Available multispectral satellite imagery (e.g., Landsat satellite imagery from the U.S. Geological Survey [USGS] public web archives) was used to map shallow-water bathymetry in a GIS environment. Various algorithms for bathymetry extraction were evaluated and the output compared to a reference data set over the coastal study site in Massachusetts. A Monte Carlo method was used to assess the uncertainty in the satellite-derived bathymetry. The final version of the procedure was tested over selected study sites in Nigeria and Belize that had been identified as in critical need of updated hydrographic surveying. Soundings from available nautical charts in the area were used to simultaneously transform the algorithm output to quantifiable depths and to reference them to the chart datum.



## Satellite-Derived Bathymetry

The spectral radiance received at an optical sensor over optically-shallow coastal waters is a function of atmospheric transmittance, sea surface reflectance, scattering and absorption in the water column, and substrate reflectance. A typical multispectral sensor contains several channels. Each channel captures a broad (70–150 nm wide) spectral range. Collectively, the channels span the visible through infrared portions of the electromagnetic spectrum. Light transmittance through the water column varies as a function of wavelength. The spectral range of sunlight that penetrates seawater to appreciable depths is typically between 350 nm

(ultraviolet-blue) and 700 nm (red), depending on the water clarity depth (Jerlov 1976; Mobley 2004). Sunlight at wavelengths greater than 700 nm (near infrared) has very low transmittance in seawater. As a result, these water areas are observed as very dark in the near-infrared (800–900 nm), making them useful in delineation of the land/water boundary in coastal regions (Robinson 2004; Jensen 2007). In the visible bands that penetrate the water column, an exponential attenuation of radiance as a function of both depth and wavelength provides the fundamental principle for depth estimation.

In order to retrieve depth information, corrections for spectral contributions from the water column, atmospheric effects, and sea surface reflections are applied to the spectral imagery. Several approaches have been developed for satellite-derived bathymetry. These approaches broadly fall into three categories:

- Analytical methods that are simplified radiative transfer models designed for a specific data set (Lyzenga 1978, 2006; Philpot 1989; Frener et al. 2012);
- Optimization approaches that assume vertically invariant water column and bottom conditions and that require either fixing all but one parameter, or solving several spectral parameters simultaneously. A subcategory includes ratio approaches that derive bathymetry based on the log ratio (or ratio of logs) of two bands (Dierssen et al. 2003; Stumpf et al. 2003; Vanderstraete et al. 2006; Su et al. 2008); and
- Look-up tables (LUT) that use a comparative method for bathymetry classification based on large database generated from radiative transfer models (Louchard et al. 2003; Bramante et al. 2013). Typically, different classifiers are used in the LUT approach to determine depth. However, neural networks have also been investigated as an empirical method to determine depth (Sandidge and Holyer 1998).

A typical assumption made for a simplified radiative transfer model approach is that the bottom is a Lambertian surface. This can provide a good approximation for some bottom surfaces (e.g., sand) but can cause errors in the computed water level radiance of up to 10% for other bottom surfaces (Mobley et al. 2003; Philpot et al. 2004). The optimization approach generally assumes a uniform bottom reflectance and water attenuation. This assumption implies that any changes in either of these environmental parameters are minor with respect to the depth calculation. Hydrographic communities can use COTS GIS software, such as *ESRI ArcMap* (Powell et al. 2009) to develop a ratio transform algorithm based on an optimization approach. This can yield a robust solution that does not require sampling the environment or generating a database.

While only the analytical methods make explicit use of a radiative transfer model, the mathematical basis for all three general approaches involves modelling the exponential decay of solar radiation in the water column as a function of the diffuse attenuation coefficient $K(\lambda)$ and depth, $z$ (Jerlov 1976; Mobley 2004). As described by Philpot (1989) and Maritorena et al. (1994), the observed radiance in shallow waters can be expressed as:

$$L_{obs} = (L_b - L_w) \cdot e^{-2K(\lambda) \cdot z} + L_w \tag{1}$$

where $L_{obs}$ is the observed radiance, $L_b$ is the radiance contribution from the bottom, and $L_w$ is the observed radiance over optically deep waters with no bottom contribution. As a result, only a subset of the spectral range from the downwelling irradiance reaches the bottom and is reflected back. The optically deep waters yield optical observations that contain mainly radiance from scattering in the water column while the radiance contribution from the bottom is negligible. The depth limit using satellite-derived bathymetry algorithms is determined by the extinction depth, which is the maximum depth that the light can penetrate

the water, ($L_{obs} \rightarrow L_w$). Areas deeper than the extinction depth will show an almost constant value that represents only the water column.

The ratio transform approach utilizes two bands to reduce the number of parameters required to infer depth (Stumpf et al. 2003). Based on the assumption that the water column is uniformly mixed, the ratio of two bands will maintain a near-constant attenuation value that is the difference of the diffuse attenuation coefficient values at two different wavelengths. The concept underlying the ratio transform approach is that bottom radiance of one band will decay faster with depth as compared to the other band. As a result, the ratio between the two bands will vary with depth. Two of the more well-known and commonly used band ratio algorithms were developed by Dierssen et al. (2003) and Stumpf et al. (2003). Dierssen et al. (2003) used a log-difference concept to derive bathymetry in turbid waters and found a strong attenuation in the red band and a relatively weak attenuation in the green band will produce a ratio that is correlated with the bathymetry. The results showed a linear relationship between the green/red (555 nm/ 670 nm) ratio and single-beam echosounder depth measurements, where gain, $m_1$, and offset, $m_0$, are empirically determined:

$$z = m_1 \cdot \left[ ln\left(L_{obs}(\lambda_i)\right) - ln\left(L_{obs}(\lambda_j)\right)\right] + m_0 = m_1 \cdot ln\left(\frac{L_{obs}(\lambda_i)}{L_{obs}(\lambda_j)}\right) + m_0 \qquad (2)$$

Stumpf et al. (2003) used a log-ratio approach with blue and green bands. Typically in coastal conditions, light in the blue wavelengths (400–500 nm) attenuates faster with depth than light in the green wavelengths (500 to 600 nm) (Jerlov 1976). The Stumpf et al. (2003) algorithm is able to reduce the errors associated with varying albedo in the atmosphere, water column and the seafloor because both bands are affected similarly. Accordingly, the change in ratio between bands is affected more by depth than by bottom reflectance (Stumpf et al. 2003). Depth can then be derived using the following equation, where the gain and offset are empirically determined, as in the Dierssen approach:

$$z = m_1 \left(\frac{ln\left(L_{obs}(\lambda_i)\right)}{ln\left(L_{obs}(\lambda_j)\right)}\right) - m_0 \qquad (3)$$

Philpot (1989) emphasized the challenge in the linear transform approach to retrieve accurate values for the water column and the seafloor optical properties. As a result of the linear transform approach being loosely constrained, the inversion calculations can fail to provide accurate depth values when the simplified assumptions (e.g., homogeneity of water column parameters) are not satisfied. Each satellite image, even over the same site, requires different constants and optical properties. In this study, only the ratio transform algorithms were evaluated. The ratio transform algorithms were determined to be an easier implementation for national hydrographic offices because these algorithms require fewer constants and no optical properties to determine bathymetry. The Stumpf et al. (2003) and Dierssen et al. (2003) satellite-derived bathymetry algorithms were both evaluated over a well-controlled environment.

## Methodology

### *Data Sets*

Based on the studies mentioned in the previous section, this study found that the most appropriate approach for satellite-derived bathymetry in hydrographic offices with limited

resources is the ratio transform approach. Although the ratio transform approach was developed over relatively clear waters (average diffuse attenuation coefficient ranges between 0.03 $m^{-1}$ to 0.05 $m^{-1}$), a satellite-derived bathymetry procedure was also tested in turbid waters. The key steps in the procedure can be grouped into preprocessing, water separation, spatial filtering, applying the bathymetry algorithms, and referencing the bathymetry to the chart datum. The northern coast of Cape Ann, Massachusetts (USA) was used as the calibration site to evaluate the different options within each step and validate the final bathymetric product. The specific site location was selected due to its challenging ocean optics conditions. New England coastal waters have average diffuse attenuation coefficient ranges between 0.1 $m^{-1}$ to 0.2 $m^{-1}$ and substrates that vary from sand and mud to sediments containing shells and rocky outcrops (Pe'eri et al. 2011). The area is a low-energy wave environment with a tidal range of about 2.5 m. The physiographic structure along the shore lines and inner shelf are controlled by the structure of the underlying bedrock formation (Barnhardt et al. 2007).

Landsat imagery was selected as the input imagery for the satellite-derived bathymetry procedure. Because Landsat imagery is freely available in many regions of the world, it is an attractive option for hydrographic surveying offices in developing nations. The Landsat imagery was obtained from public archives: http://earthexplorer.usgs.gov. The Enhanced Thematic Mapper plus (ETM+) in the Landsat satellite platform collects eight bands of imagery with a ground swath of 185 km at a ground resolution of 28.5 m for most bands (the panchromatic band and the thermal infrared band have a different ground resolution). The large swath of the Landsat imagery can potentially cover a nautical chart at a scale of 1:50,000 with a single image. For this study, only four of the eight bands were investigated: blue (420–520 nm), green (530–610 nm), red (630–690 nm), and near-infrared (780–900 nm). The Landsat imagery was downloaded as ortho-rectified images referenced to WGS84 (original realization). The stated spatial accuracy of the imagery is better than 50 m (USGS 2006). The Landsat image selected for the calibration study site was collected at 15:16 UTC just before the end of flood tide on 27 September 2000.

Each bathymetric model produced from the different procedure configurations was compared to an Airborne Lidar Bathymetry (ALB) survey that was collected in 2007 by the U.S. Army Corps of Engineers. Although the native resolution of the Lidar data would have supported gridding at 3 m resolution, for purposes of this study, the Lidar measurements were gridded at the Landsat image resolution (28.5 m). Bathymetry was derived using blue-green and red-green band pairs. In addition to the algorithm evaluation, the use of spatial filters in the preprocessing procedures was also evaluated. Although this process is intended to validate the chart depths, selected chart soundings were used to reference the satellite-derived bathymetry to the chart datum. These soundings are used as control points for the algorithm results to calculate the gain and offset that are applied to the ratio transform output. Although the instantaneous water level at the time of satellite image acquisition is very unlikely to coincide with the chart datum (e.g., Mean Lower Low Water [MLLW] or Lowest Astronomical Tide [LAT]), there is no need to measure the tide height during the image acquisition because this is automatically accounted for using control points that are selected from a nautical chart to determine the transformation parameters. Differences in water levels over small spatial extents are usually well approximated as a vertical offset and do not impair the linear relationship between chart soundings and ratio algorithm output. Therefore, the procedure eliminates both the need for tide-coordinated imagery and for tide correctors. In the U.S. calibration site, chart soundings from two NOAA charts were used (NOAA 2009a, b): 1) NOAA Chart 13279 Ipswich Bay to Gloucester Harbor (scale 1:20,000) and 2) NOAA Chart 13278 Portsmouth to Cape Ann (scale 1:80,000). The

horizontal datum for both charts is North American Datum 1983 (NAD 83). The depth soundings are in feet and are referenced to the MLLW tidal datum. Hydrographic surveys in the areas covering the test site were conducted between 1940 and 1969 by the U.S. Coast and Geodetic Survey, now NOAA's National Ocean Service (NOS). The survey used single beam echo sounders for depth and primarily visual aids for positioning achieving partial bottom coverage along sounding profiles.

Data availability is an important factor. Landsat 7 has operated successfully since April 1999. However, its operations have been marred by a faulty scan line corrector since June 2003. This flaw has made coastal mapping with the satellite problematic. A new Landsat satellite, Landsat Data Continuity Mission (LDCM), was launched on 11 February 2013. In addition, satellite imagery at higher pixel resolution can be purchased from commercial companies (e.g., IKONOS, QuickBird, and WorldView). The substitution of Landsat 7 imagery with imagery from any of these other satellites is straightforward. However, it is important to identify the green and blue bands that provide the most range using the band ratio algorithm.



### *Key Steps in the Optic-derived Bathymetry Procedure*

*Preprocessing.* Based on the chart's geographic location, a search was conducted in the USGS archives for Landsat 5 and Landsat 7 imagery. After reviewing the different available scenes in a 'quicklook view' mode (i.e., low-resolution imagery), only images with cloud coverage less than 10%, and free of glint over the water were chosen for the calibration site. These images were downloaded from the USGS website into an ArcMap project, where the imagery from each band was saved in a TIF format.

A mask polygon of the submersed areas was generated based on the water separation step. The polygon was subsequently used to extract only the water body from the Landsat imagery in the red, green, and blue (RGB) bands. Due to the presence of "speckle noise" in the Landsat imagery, the subset RGB was saved with and without filtering in the spatial domain. The cause of the speckle is unclear. It may be due to memory effects, scan-correlated shift and coherent noise (Vogelmann et al. 2001). Some of the spatial filters that were evaluated included: low-pass, mean, median, minority, majority, minimum and maximum.

*Clouds, sun glint, and water separation.* Radiometric calibration is an important aspect of pre-processing for bathymetry estimation. In this work, rigorous atmospheric correction was unnecessary, due to the use of the band ratio method of depth estimation. Instead, cloud cover was removed using the near infrared (NIR) band. As water is close to opaque in the NIR portion of the electromagnetic spectrum, the water appears dark (low digital values) in band 4 of the Landsat imagery (Figure 1a). The dark areas in the NIR band contrast sharply with the dry land areas that reflect well in the NIR and appear bright (high digital values). Clouds also reflect well in the NIR. As a result, the histogram of the NIR band over a coastal area is bimodal with two modes corresponding to land and water regions (Figure 1b). In this study, a threshold value between the two distributions was used for separating land (and clouds) from water in the NIR band. The exact threshold value was determined manually based on profiles in the NIR band that crossed over land and water features (Figure 1c). It is important to note that this land/water interface is the instantaneous shoreline at the acquisition time of the Landsat imagery. The bathymetry will be vertically corrected to the chart datum (regardless of water level to which this instantaneous shoreline corresponds). Cloud shadows and sun glint on the water surface that might be present in the images are

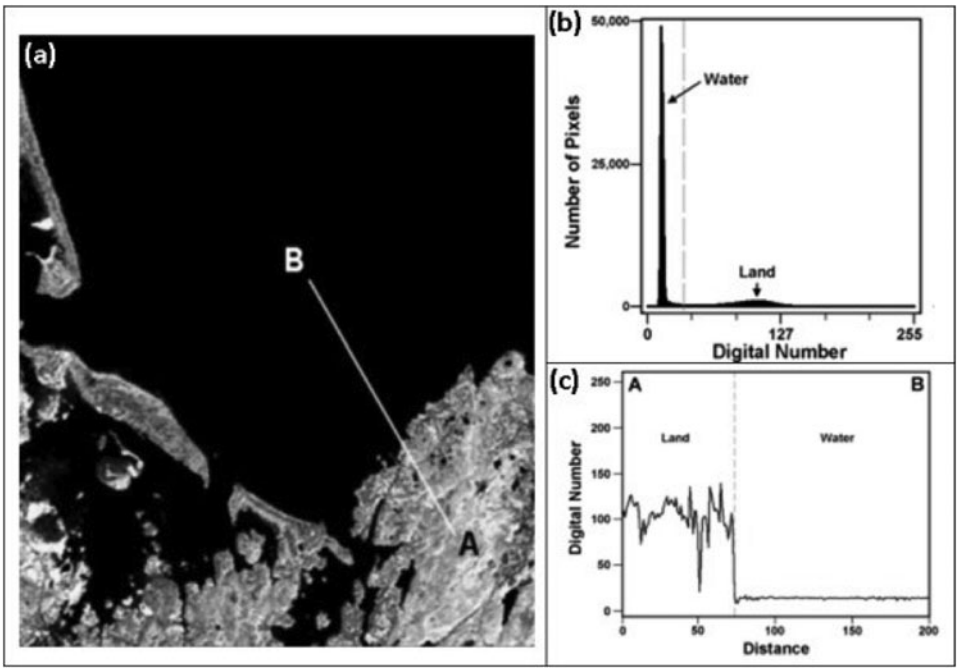


**Figure 1.** (a) Infrared Landsat image (band 4) of Cape Ann, MA, USA; (b) histogram of infrared Landsat image (a) representing the distribution of pixels as function of the digital number value; and (c) Profile plot of section A-B overlaid on the infrared Landsat image (a) where the distance is in pixels.



removed using the Hedley et al. (2004) approach:

$$L'_{obs}(\lambda_i) = (L_{obs}(\lambda_i)) - b_i \cdot ((L_{obs}(NIR)) - Min\,(L_{obs}(NIR))) \quad (4)$$

where the pixel value in band i, $L_{obs}$ $(\lambda_i)$, is reduced by the product of regression slope, $b_i$, and the difference between the pixel NIR value, $L_{obs}$ *(NIR)*, and the ambient NIR level, *(Min(*$L_{obs}$ *(NIR))*. The result is a radiometrically corrected pixel that essentially represents the pixel value of a given band without glint or shadows.

*Applying the bathymetry algorithm and vertical referencing.* The Dierssen et al. (2000) and Stumpf et al. (2003) algorithms (Eqs. (2) and (3), respectively) were used to generate models of the blue/green and green/red bands for the unfiltered and filtered images. This resulted in eight possible procedure configurations for each algorithm: unfiltered and filtered blue/green bands, and unfiltered and filtered green/red bands. In order to calculate the gain and offset values for Eqs. (2) and (3), the algorithm results were compared and correlated to the chart soundings (Figure 2). The referencing step includes three substeps:

a. **Selecting reference soundings.** Typically, the two main considerations for selecting reference soundings are 1) the chart source diagram that indicates both the survey period and the survey technology and 2) a visual correlation between the satellite-derived bathymetry and the chart contours and/or soundings. In this study, several procedure configurations were investigated to determine only those chart soundings that are reliable enough for the empirical calculations. These depth

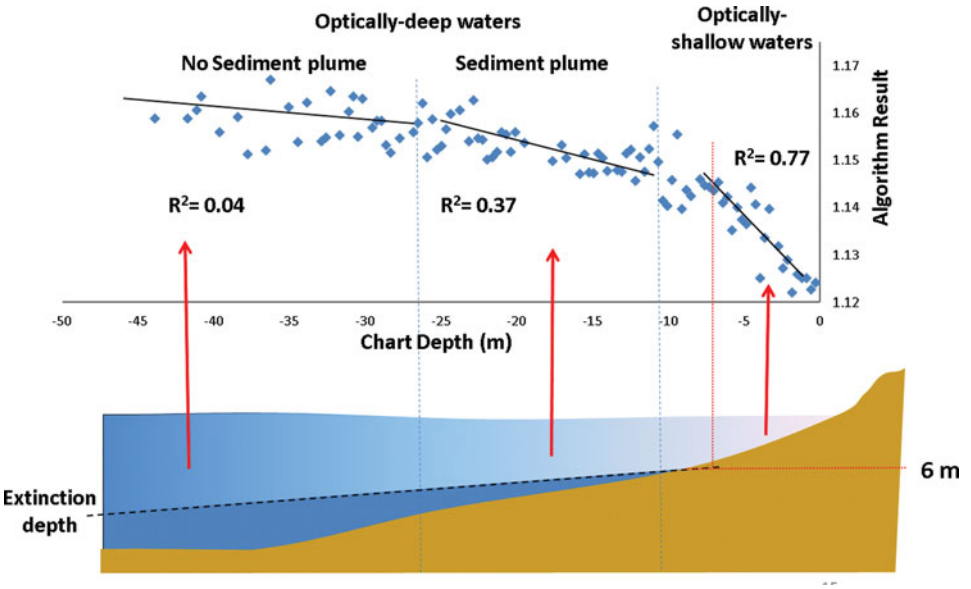


**Figure 2.** A schematic illustration of the statistical analysis at the calibration site using the blue-green Stumpf et al. (2003) algorithm with a low-pass filter. Top part of the image shows the scatter plot of the algorithms results as a function of the chart sounding (MLLW). The bottom part of the image provides a possible explanation for the algorithm results and their relation to the depth of extinction.



soundings were then compared to the ALB reference data set. As charts are compiled from multiple historical hydrographic surveys, reference soundings should be selected over areas in which the charted seafloor morphology shows visual correspondence with the algorithm result. Additional soundings should be selected from the chart over optically deep waters (i.e., seafloor morphology cannot be recognized in the algorithm result) in order to determine the extinction depth. In cases of multiple satellite images, areas with overlapping soundings should be selected for consistency.

b. **Identifying the extinction depth.** The algorithm model results were compared with the ALB data set and the chart soundings at coincident points based on the location of the chart soundings. Only two soundings are needed for calculating the gain and offset. However, additional soundings provide redundancy (i.e., an overdetermined system), such that statistically optimal (in the least squares sense) estimates of the gain and offset parameters can be obtained. In this study, multiple depth measurements from the satellite-derived bathymetry and ALB bathymetry datasets with the same chart sounding depth were averaged into a single value. The averaged values of the satellite-derived bathymetry were plotted against the chart soundings and the ALB bathymetry. This was used to identify the boundary between the areas where the seafloor contributes to the recorded pixel values (i.e., optically shallow areas) from those areas where the only contributions are water color and suspended particulates (i.e., optically deep areas). Based on a visual inspection of the depth measurements, other depth boundaries were

also determined. The ALB data set was used to validate the results using chart soundings.

c. **Statistical analysis.** Based on the band ratio approach as seen in Eqs. (2) and (3), areas shallower than the extinction depth show a linear relationship between the reference bathymetry and the algorithm results. Areas deeper than the extinction depth do not show a clear correlation between the reference bathymetry and the algorithm results and will break from the linear trend of the optically shallow waters. A regression analysis was used to indicate the linearity between the data sets. The calculated parameters in the regression analysis included $R^2$ (the coefficient of determination), gain, and offset. Based on the highest correlation ($R^2$ closest to 1), the best procedure configuration was selected. Figure 2 illustrates the statistical analysis of over the calibration site using the blue-green Stumpf et al. (2003) algorithm with a low-pass filter. Three zones are identified from plotting the algorithm's results as a function of the chart sounding (Figure 2): bathymetric region (i.e., the optically shallow waters) ($R^2 = 0.77$), optically deep waters that contain a sediment plume ($R^2 = 0.37$), and optically deep waters that are relatively clear ($R^2 = 0.04$). From an operational perspective, it is important to evaluate bathymetric regions based on assigned navigational depths. This is especially critical between depths that are not for navigation (i.e., too shallow for navigation) and shallow-navigational water. These depth ranges are separated based on the channel and anchorage depths that lead to ports in their vicinity.



### *Uncertainty Estimation*

The IHO S-44 standards call for "a statistical method, combining all uncertainty sources" for the determination of the "total vertical uncertainty" (TVU) (IHO 2008). Even if the data do not meet the TVU specifications of the IHO survey orders (i.e., Special Order, Order 1a, 1b, or 2), computed and reported uncertainties should accompany the survey data. These uncertainty estimates are critical to evaluate if the survey data are suitable for various applications. In theory, it is possible to analyze the uncertainties in depths obtained from the Stumpf algorithm through conventional (i.e., analytical) uncertainty propagation methods. From Eq. (3), an analytical uncertainty propagation (e.g., Mikhail 1976; JCGM 2008a) leads to the following expression for depth uncertainty using $L_b$ and $L_g$ as the blue and green bands in the Landsat imagery:

$$\sigma_Z = \left(\mathbf{J}\boldsymbol{\Sigma}\mathbf{J}^T\right)^{1/2} \tag{5}$$

where

$$\mathbf{J} = \begin{bmatrix} \dfrac{\partial Z}{\partial m_0} & \dfrac{\partial Z}{\partial m_1} & \dfrac{\partial Z}{\partial L_b} & \dfrac{\partial Z}{\partial L_g} \end{bmatrix} \tag{6}$$

$$\boldsymbol{\Sigma} = \begin{bmatrix} \sigma_{m_0}^2 & \sigma_{m_0 m_1} & \sigma_{m_0 L_b} & \sigma_{m_0 L_g} \\ \sigma_{m_0 m_1} & \sigma_{m_1}^2 & \sigma_{m_1 L_b} & \sigma_{m_1 L_g} \\ \sigma_{m_0 L_b} & \sigma_{m_1 L_b} & \sigma_{L_b}^2 & \sigma_{L_b L_g} \\ \sigma_{m_0 L_g} & \sigma_{m_1 L_g} & \sigma_{L_b L_g} & \sigma_{L_g}^2 \end{bmatrix} \tag{7}$$

However, this approach to uncertainty analysis imposes several complications. First, it should be noted that $m_0$ and $m_1$ are not directly measured quantities with easily quantifiable standard deviations, but rather coefficients of a linear regression of reference depths on the

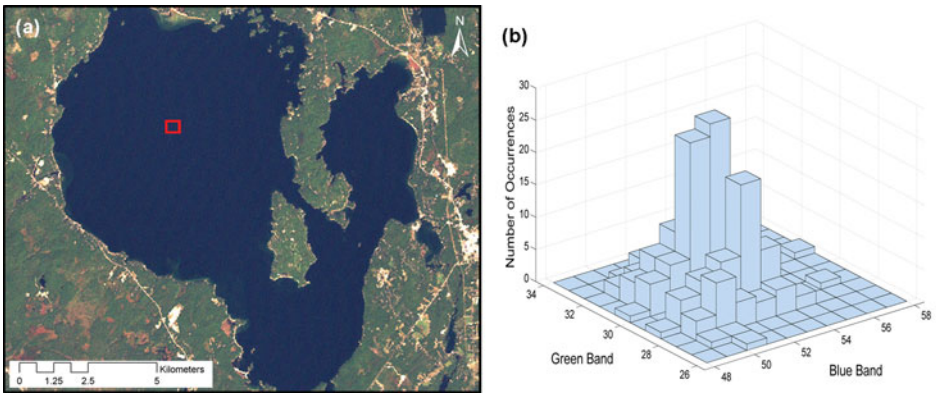


**Figure 3.** (a) Homogeneous image subset (14 by 16 pixels) used in estimating parameters of joint probability distribution of blue and green image pixel values near the calibration study site. (b) Corresponding bivariate histogram of the blue and green bands in DN.



ratio of logs of the blue and green image bands. In this study, the set of reference depths, $\{Z_{ref}\}$, consists of user-selected chart soundings from the most recent (or most reliable) hydrographic survey in the project area. An additional complicating factor to obtain a reliable estimate of the covariance matrix, $\mathbf{\Sigma}$, is that none of the off-diagonal elements can be safely assumed to be zero.

A commonly used alternative to analytical uncertainty analysis, which avoids some of the complications and limitations of the analytical approach, is to employ a Monte Carlo (MC) method (JCGM 2008b; Papadopoulos and Yeung 2001). One option would be to use MC to obtain estimates of the elements of $\mathbf{\Sigma}$ in Eq. (8) and then proceed analytically. However, a simpler and more logical approach is to sample from the distributions that model the uncertainties in the initial input parameters to the Stumpf algorithm (green and blue image pixel values and reference soundings) and to propagate those uncertainties through to the final output of the Stumpf algorithm (i.e., depth).

The necessary input for the MC method comprises the parameters of the probability distributions of the input variables used to determine satellite-derived depths via the Stumpf algorithm: $Z_{ref}$, $L_b$, and $L_g$. The uncertainty in $Z_{ref}$ is modelled as a zero-mean, Gaussian random variable. Because the two spectral bands are likely to be correlated to some degree, the uncertainty in $(L_b, L_g)$ is modelled as a bivariate Gaussian distribution, $\mathcal{N}(\mathbf{0}, \mathbf{\Sigma}_{\mathrm{L}})$.

The NOAA hydrographic survey data that constitute the reference soundings for the Massachusetts calibration site were collected between 1940 and 1969, and cannot be safely assumed to meet current IHO S-44 Order 1a standards (IHO 2008). Instead, an adherence to the first set of IHO standards promulgated in 1968 was assumed. The quoted standard was 0.3 m (assumed to be a $1\sigma$ value) in depths of 0–20 m. The tide corrector accuracy was quoted by the charting agency as one-half the sounding accuracy standard. Summing these two values in quadrature gives: $\sigma_{Z_{ref}} = 0.34$ m.

Through scatter plots of the blue and green bands that were produced over homogeneous areas, it is possible to obtain the parameters of the bivariate distribution of the blue and green band pixel values. For the calibration study site, a small subset of the central portion of a still, optically deep lake (Sebago Lake, Maine, Figure 3a) was selected as the homogeneous image region. Using the data in the bivariate histogram of Figure 3b to estimate the

parameters of the joint distribution, yields:

$$\Sigma_L = \begin{bmatrix} \sigma^2_{L_b} & \sigma_{L_b L_g} \\ \sigma_{L_b L_g} & \sigma^2_{L_g} \end{bmatrix} = \begin{bmatrix} 2.09 & 0.17 \\ 0.17 & 1.51 \end{bmatrix} \tag{8}$$

where the units of the variances and covariances are the squares of the units of the pixel values that can represent at-sensor radiance, spectral radiance, or reflectance. Unitless digital values, provided in the Landsat imagery, represents one of these three radiometric cases, depending on the level of radiometric calibration applied in preprocessing.

The MC algorithm for uncertainty estimation was implemented in MATLAB. The input includes: 1) each green and blue image band combination (i.e., actual image data) for pixels for which the depth uncertainty will be estimated, 2) the set of reference soundings, 3) blue and green band image pixel values at the locations of the reference soundings, and 4) parameters of the distributions described above. The algorithm then proceeds as follows:

- For $i = 1$ to number of MC trials
  - i Perturb the input values by random amounts, which are obtained by sampling from the probability distributions modelling their uncertainties. Through a least squares adjustment, compute $m_0$ and $m_1$
  - ii Compute output depth from the Stumpf algorithm
- After all runs are completed, plot the distribution of output depths
- Compute summary statistics (mean and standard deviation) for the output depths in the area of interest.

Figure 4 shows a histogram of output depths obtained from this MC TPU algorithm for a particular example pixel, in a case were the baseline (unperturbed input) yields an output depth of ~4.7 m. The estimate of the depth uncertainty obtained using this MC method for

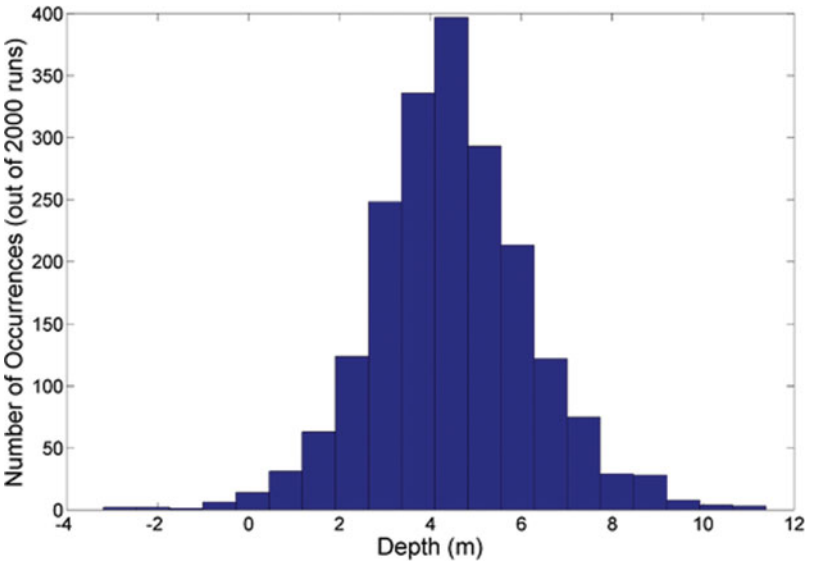


**Figure 4.** Example histogram of output depths from MC uncertainty analysis algorithm for the calibration study site.

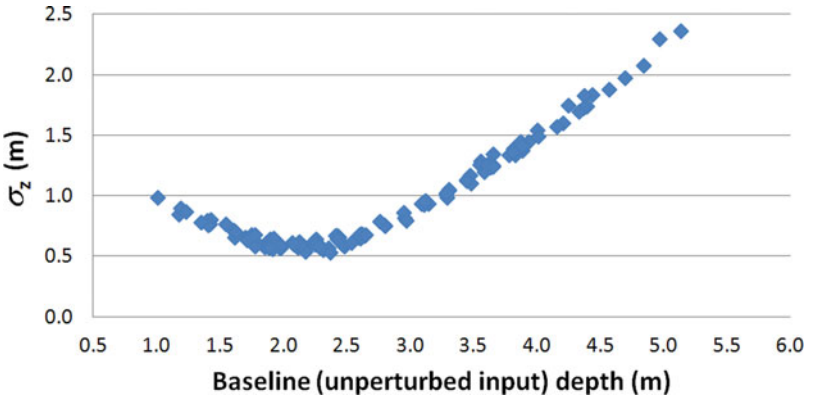


**Figure 5.** Estimated depth uncertainty from the MC algorithm as a function of depth. Minimum depth uncertainty values occur at ~2.0–2.5 m.



the portion of the Massachusetts test site in which the reference soundings are located is $\hat{\sigma}_Z = 1.79\,m$. This result agrees with the empirically-determined uncertainty for this site to within ~2%.

An additional component of testing the MC algorithm involved ensuring that the model behaves as expected as inputs are varied. For example, estimated depth uncertainty as a function of depth for the Massachusetts calibration site is shown in Figure 5. As can be seen in the figure, there is a "sweet spot" at ~2.2 m water depth, where the uncertainty reaches a minimum. The shape of this curve can be explained in terms of the physics of the depth measurement process. At deeper depths, the integration of component uncertainties over greater optical path lengths through the water column leads to greater TPU. Meanwhile, at shallower depths, breaking waves, bubbles, and resuspended sediment lead to greater measurement uncertainty. Hence, the minimum uncertainty occurs at the intersection of two curves: one downward and one upward sloping. For the calibration site, we find that this intersection occurs at ~2.2 m. From these types of analyses, it was found that the MC algorithm results appear to correctly model the expected behavior.

It should be noted that the MC approach to uncertainty estimation used in this study does not explicitly account for uncertainty introduced by spatially varying environmental conditions. However, the algorithm could be modified to implicitly account for this by updating the method used to estimate image pixel value uncertainty. The basic approach would entail using neighborhood statistics tools that are available in common GIS packages to generate local estimates of the image pixel uncertainties for the MC algorithm. Areas of spatially varying environmental conditions would then be reflected in higher variance in image pixel values, which would propagate to greater uncertainty in the output bathymetry. While the GIS implementation is quite straightforward, initial tests show that there are some issues that need to be addressed, such as contributions from exposed features in the nearby vicinity (e.g., clouds, islands, offshore rocks, and ships). To address such issues will require more complex algorithms and/or manual (i.e., human) analysis, which is not deemed necessary in this study as the uncertainty analysis was performed for small areas of relatively uniform water.

## Study Results

To assess the performance of the different procedure configurations, elevation difference maps were generated by comparing the different satellite-derived bathymetry results to a reference bathymetry dataset from an ALB survey. The computed vertical offset used to transform the ALB data set, which contains NAD 83 (CORS96) ellipsoid heights, was 27.78 m. This value is consistent within the estimated uncertainties of the data, with the 28.33 m MLLW – NAD 83 (CORS96) datum offset obtained for this area using NOAA's Vertical Datum (VDatum) transformation utility (Myers et al. 2007). The fact that the chart soundings are shoal biased (i.e., typically represent the shallowest measurement in the vicinity) may contribute to the 55 cm difference between the computed offset and that obtained from VDatum.

A statistical analysis of the difference maps showed that the procedure configuration using the blue-green band ratio with a low-pass filter provides the most accurate measurement of the bathymetry. The blue-green band ratio with a low-pass filter also presents the morphological features most clearly. The correlation values in the areas overlapping the ALB dataset showed very high correlation values. The mean depth difference of the satellite-derived bathymetry to the ALB data set is 0.30 m with a standard deviation of 1.83 m. After validating the algorithm results with the ALB data set, the extinction depth with respect to the chart datum was calculated from the scatter plots of algorithm results versus depth. The extinction depths were calculated to be around 6 m MLLW for all the configurations.

These results indicated that the depth differences were less than 2 m for most areas (Figure 6). The difference was greater than 4 m in only a few instances. This higher difference may be due to turbidity caused by along shore currents and/or waves over features with steep boundaries (e.g., channels within a sandy seafloor or rocky outcrops and boulder glacial deposits in the vicinity of flat lying sediments). In both cases, there is the potential that sediment was suspended above the seafloor which increased the turbidity of the water. While it may be impossible to determine the cause of the turbidity without further information (e.g., wave height at the time of imagery acquisition), it should be noted that the general effect of turbidity is a false shoaling. This is important for hydrographic surveying offices, as false shoaling leads to more conservative soundings and, therefore, is generally preferable from a charting perspective.

Differences between the datasets were also observed in the northwest part of the study site at water depths greater than 6 m, which is about the depth of extinction for the image. This vertical difference may be caused by changes to the seafloor morphology over the time difference between the data collection times of the ALB and satellite images. Furthermore, errors in the georeferencing of the two datasets could contribute to these vertical differences.

The $R^2$ values between the algorithm results of the blue-green band ratio in the bathymetric region improved (i.e., increased) by 0.28–0.34 by using the low-pass filter. Both algorithms (Stumpf and Dierssen) provide similar correlation results after applying the low-pass filter, with an $R^2$ difference of about 0.01 between the two algorithm results. Correlation results between the procedure results and the ALB data set confirm these results, where both the Stumpf and Dierssen algorithms provided the same correlation values for a blue-green band ratio using the low-pass filter. However, the results from the green-red band ratio for both the Stumpf and Dierssen algorithms were significantly lower after applying the low-pass filter, with $R^2$ values of 0.32 and 0.35, respectively. It was also difficult to identify the extinction depths from the scatter plots of algorithm results versus depth. The procedure results were further evaluated as a function of depth, where ALB

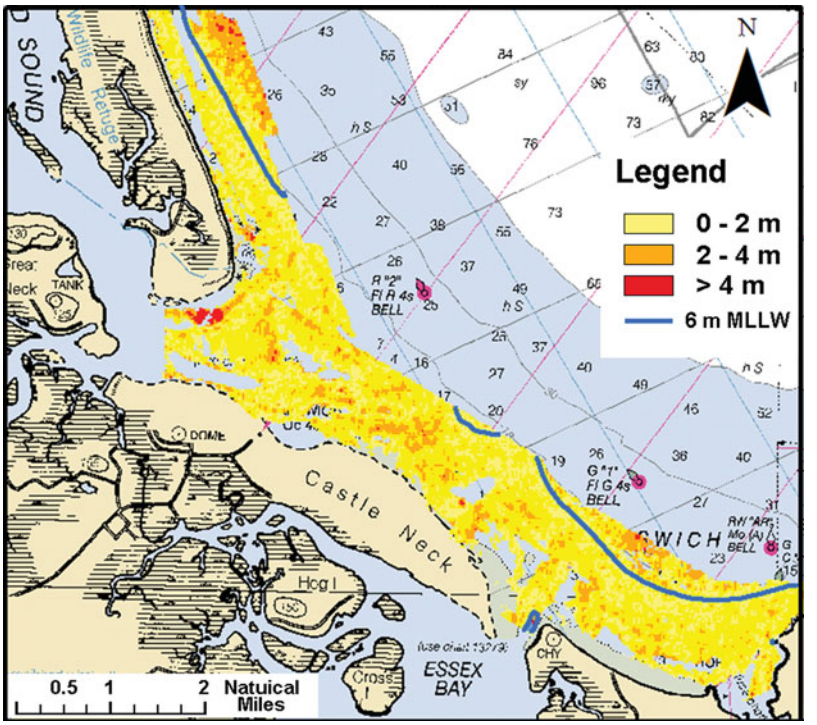


**Figure 6.** Vertical difference results between the satellite-derived bathymetry and the ALB data set over the calibration site. The 6 m MLLW contour line that represents extinction depth is marked as a blue line.

measurements were used in shallow waters (0 to −6 m MLLW) and chart soundings were used in deep waters (deeper than −6 m MLLW). The comparison results between the bathymetry from the different procedure configurations and the ALB data set showed that the low pass-filtered blue-green Stumpf algorithm performed the best based on the $R^2$ values at extremely shallow to intermediate depths. It is important to note that the correlation values were very low (0.20 – 0.30) for all procedure configurations at extremely-shallow water depths (0 to –1 m MLLW). The low performance of the algorithms at extremely shallow depths may be attributed to poor water clarity or aeration as a result of wave action in the surf zone. The algorithm results in the seaward direction represent a reduction in the concentration of the suspended sediments and not an increase in depth. Outside of the sediment plume (optically deep waters) the plot shows no correlation ($R^2 < 0.04$) with the chart soundings.

## Other Study Sites

### *Potential Applications*

With the development of a procedure to derive bathymetry from satellite imagery, chart soundings can be used as a suitable constraint to reference the satellite-derived bathymetric dataset. The highest ranking procedure configuration was used to produce shallow-water bathymetry in the coastal waters of Nigeria and Belize. These two sites were selected based on the IHO publication C-55 (IHO 2004) that identified the nautical charts of Nigeria and Belize as containing significant gaps in hydrographic survey data and resulting nautical

charts. For instance, the best available nautical charts for Nigeria (BA Chart 3321) and Belize (BA Chart 1797) show that only a small portion of the charted area was surveyed in the last 50 years. Other areas have never been adequately surveyed, or the last hydrographic survey was conducted more than 100 years ago. These nautical charts of Belize and Nigeria were used to investigate the potential applications for satellite-derived bathymetry. In particular, there is interest to develop practical satellite remote sensing methods that can be used to improve existing nautical charts for developing nations. Such applications include the production of digital elevation models (DEMs) to identify areas in the chart that are poorly surveyed or outdated.



### *Nigeria Study Site (Escravos)*

The Nigeria study site is the Escravos region and includes coastal areas near the mouths of the Escravos and Forcados Rivers located in southwest of the Niger Delta. The substrates of the study site are mainly sand and mud in a relatively high-wave environment with a tidal range of about 2.2 m. The wave action forces a strong littoral current in the northwest direction. The Escravos and Forcados Rivers discharge sediments into the area which are then transported northward by the alongshore currents. Typical of delta features, changes in the bathymetry of the Escravos and Forcados Rivers are expected. The Escravos study area is covered by BA Chart 3321 (UKHO 2000) at a scale of 1:60,000. The vertical datum of the chart soundings used to reference the satellite-derived bathymetry is LAT, and depths are given in units of meters. The horizontal datum of the chart is WGS 84 (unknown realization, presumably original), and a Mercator map projection is used. Survey periods noted in the chart range between 1910 and 2004. The historic surveys ($>$ 50 years old) were carried out by the Nigerian Ports Authority and Nigeria Marine Surveys, while the more recent data (2004) are from commercial surveys (Figure 7a).

A Landsat image acquired on 17 February 2001 at 09:47 GMT over the Escravos site was downloaded for the study. The image is characterized by 10% cloud cover that mainly affected the land area and southern coastline. Bathymetry for the Escravos site was derived according to the procedure and was referenced to the LAT chart datum (Figure 7b). Although the chart was compiled from a number of old surveys, it was possible to identify areas with the same seafloor morphological characteristics that are observed in the Stumpf algorithm result. The comparison plot between the filtered blue-green Stumpf algorithm to the chart soundings that was used to calculate the linear regression showed a good correlation ($R^2 = 0.83$). The calculated extinction depth for the image was $\sim$ 6 m with respect to LAT. Deeper areas (e.g., sediment plume waters and optically deep waters) showed a poor correlation ($R^2 = 0.03$). The depth information in the chart up to the extinction depth is considered historical in comparison to the satellite imagery collected in the last 10–15 years.

For the Nigeria study site, the depth ranges were segmented based on significant navigational depths: from 0 m to 5 m, 5 m to 30 m, 30 m to 40 m, and greater than 40 m. However, the depth of extinction for satellite-driven bathymetry was about 6 m. Thus, only the 5 m contour of the depth area layer was updated (Figure 7d). From a hydrographic perspective, the updated results from the satellite-driven bathymetry were minor. The main changes in the bathymetry were north of Escravos River and south of Forcados River, where sediment had accreted. The bathymetry change near the mouths of the Escravos and Forcados rivers that are important for navigation was a small systematic accretion that may be within the accuracy of measurement. According to the chart, the areas with the

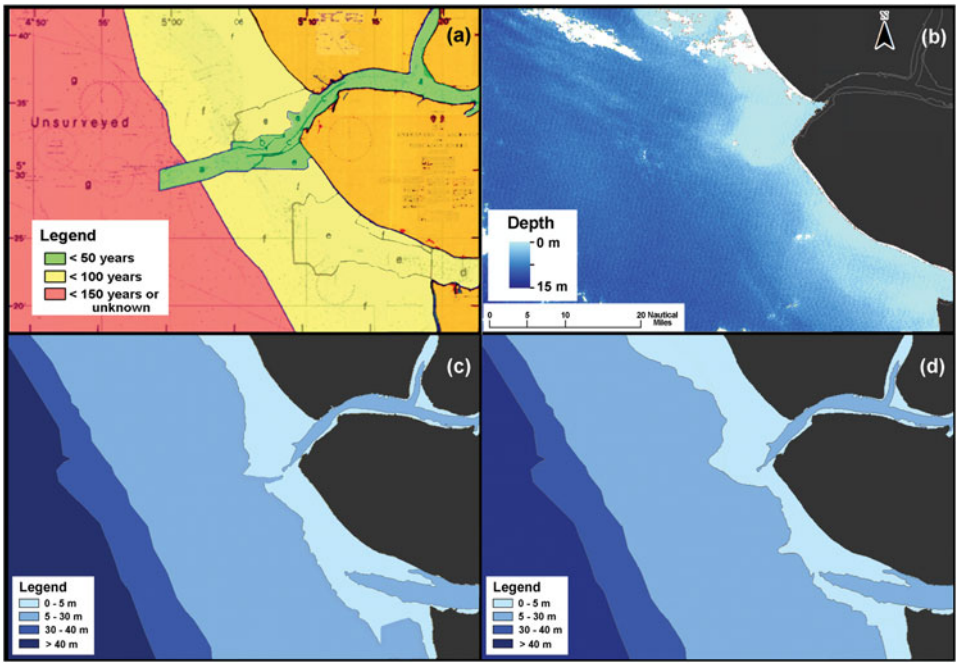


**Figure 7.** (a) British Admiralty (BA) charts overlaid with source diagram of Escravos, Nigeria (BA Chart 3321). The source diagram is color coded to show the periods of surveys used to compile the chart. (b) Satellite-derived bathymetry. (c) Significant navigational depths based on the depth sounding in BA Chart 3321. (d) Updated thematic map of the significant navigational depths using satellite-derived bathymetry (up to the extinction depth).

most significant changes in the bathymetry were last surveyed more than 100 years ago (Figure 7a).

### *Belize Study Site (Big Creek)*

The Belize study site is in the Big Creek area located on the southeast coast of Belize bounded by the Caribbean Sea to the east and Guatemala to the south. The substrates of the Belizian study site are characterized by mud, sand, and an extensive coral reef system. The area is a wave dominated environment with a tidal range of about 0.5 m. Winds coming from the northeast produce waves of about 0.3 m in amplitude. These waves generate alongshore currents setting south, where the magnitude of the current depends on the energy of the wind and angle of approaching waves. Although the rivers discharge sediments that form long barrier islands, the waters within the Inner Channel area (the area between the coastline and the reef) are considered clear. The Belize study area is covered by the BA Chart 1797 (UKHO 1989) at a scale of 1:125,000. The horizontal datum of the chart is WGS84, and a Mercator map projection is used. The chart soundings are presented in meters and referenced to LAT. Survey periods in the chart range from 1834 to 1991. These surveys were carried out by the British Government Surveys, while the more recent surveys (1988–1991) are from commercial surveys (Figure 8a).

The charted area of the Big Creek study site is larger than the Nigerian study site and required four overlapping Landsat satellite images to cover the entire chart. These

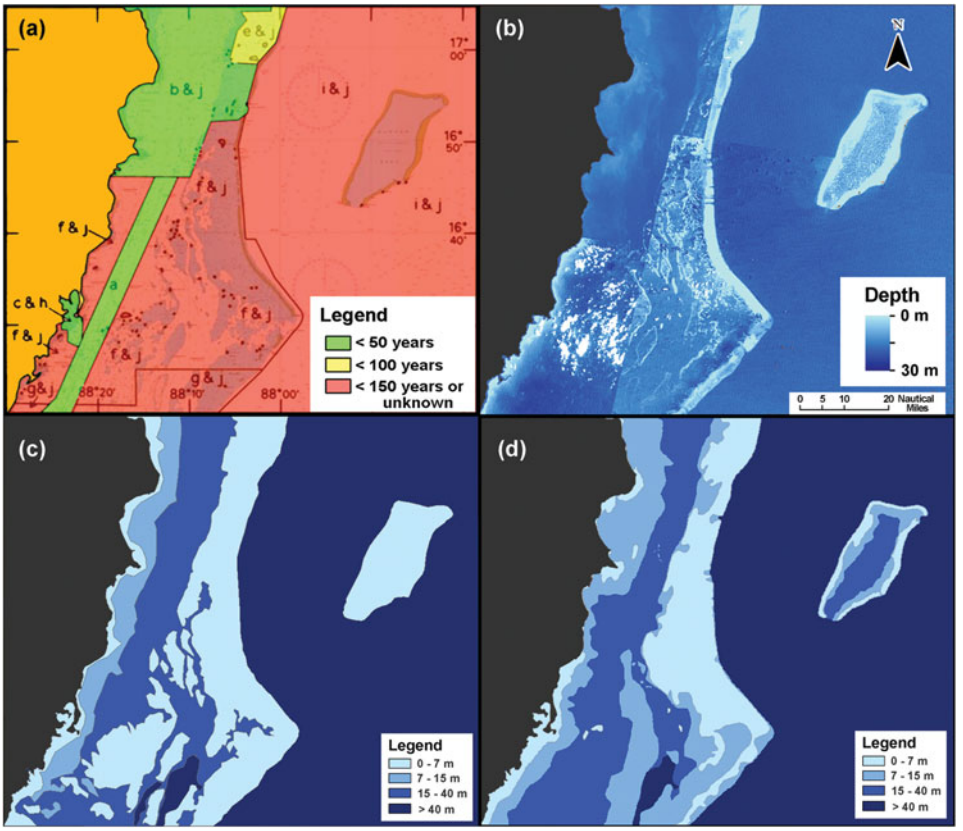


**Figure 8.** (a) BA charts overlaid with source diagram of Big Creek, Belize (BA Chart 1797). The source diagram is color coded to show the periods of surveys used to compile the chart. (b) Satellite-derived bathymetry. (c) Significant navigational depths based on the depth sounding in BA chart 1797. (d) Updated thematic map of the significant navigational depths using satellite-derived bathymetry (up to the extinction depth).

images were collected at different times (Table 1); consequently, each image was processed separately. Bathymetry for the Big Creek site was also derived according to the procedure and was referenced to LAT chart datum (Figure 8b). In addition, the chart included many incomplete and unsurveyed areas and chart soundings that overlap with eastern and south-eastern Landsat images were considered reliable. Accordingly, soundings were selected only from surveyed areas that have been stable (i.e., consistent with the satellite-derived bathymetry models) over time. An $R^2$ value of 0.85 and 0.80 was calculated only for the north-eastern (image 1) and south-eastern (image 3) Landsat images (Table 1). The bathymetric model derived from these was used to generate a control point to derive the bathymetric models for the north-western (image 2) and south-western (image 4) from Landsat images. All bathymetric models were merged together into one seamless surface (Figure 8b). In places of surface overlap, the bathymetric surface with a higher $R^2$ value was given preference. Due to the limited accuracy of the gain and offset calculation from the chart soundings, a surface discontinuity occurred in some places as a result of the different depth values that were calculated (typically, up to $\pm$ 2 m offset).

**Table 1**
Landsat imagery collected over the Belizian study site. A coefficient of determination ($R^2$) was calculated between satellite-derived bathymetry models and chart soundings that are stable over time

| Image number | Location on the chart | Acquisition Date | Extinction Depth (LAT) | $R^2$ |
|---|---|---|---|---|
| 1 | Northeast | 27 December 1989 | 24 m | 0.85 |
| 2 | Northwest | 08 November 2001 | 21 m | N/A |
| 3 | Southeast | 29 March 2003 | 24 m | 0.80 |
| 4 | Southwest | 30 April 2000 | 17 m | N/A |



Similar to the Nigerian site, the depth ranges in Belize were segmented based on assigned navigational depths: shallower than 7 m, from 7 m to 15 m, from 15 m to 30 m, and deeper than 40 m (Figure 8c). Based on the extinction depths of the Landsat images that range between 17 m to 24 m relative to LAT, only the 7 m and 15 m contours of the depth area layer were updated using the satellite-derived bathymetry (Figure 8d). Changes in bathymetry between the two datasets are the most noticeable in the shallow waters along the northeast section of the chart that is a part of the Inner Channel geographic zone of the barrier reef. Although this area was surveyed in the past 50 years (Figure 8a), many of these surveys were "incomplete." The change in bathymetry over this area is important for marine navigation planning, and depth differences between the chart and satellite imagery indicate some uncharted hazardous areas for navigation. In addition, bathymetry is now

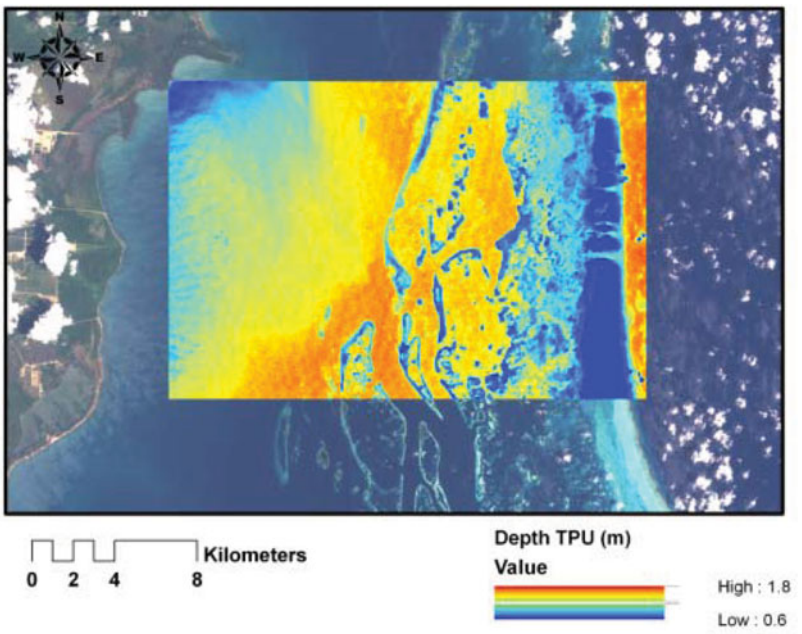


**Figure 9.** Gridded uncertainty estimates for a portion of the Belize site. The colors represent depth TPU in meters, as estimated by the Monte Carlo algorithm.

available for areas that were too dangerous to survey by ships and as a result, were never surveyed (southern part of the barrier reef and a neighboring atoll, Glover Reef). Currently, many of these areas are presented on the chart using generalized contour lines that identify a general depth or the location of exposed coral reefs.

To assess the uncertainty in the derived bathymetry for the Belize site, the MC simulation method was applied. The reference soundings from the historical surveys could not safely be assumed to meet current IHO Order 1a standards, or even the earlier (1968) standards. IHO Order 2 was assumed instead, yielding $\sigma_{Z_{ref}} = 0.51$ m. Also, the parameters of the joint distribution of the blue and green band pixel values needed to be assessed for the image from which the bathymetry was derived. The final output uncertainty estimate for the satellite-derived bathymetry in this site was: $\hat{\sigma}_Z = 1.33\,m$. The spatial variation of the uncertainty was assessed by generating uncertainty surfaces (Figure 9). The uncertainty surface was created by gridding the output of the Monte Carlo TPU estimation algorithm.

The mean uncertainty for the Belize site was slightly lower than that for the calibration site. This might seem counterintuitive because the uncertainty in bathymetry retrieval generally increases with depth (Figure 9), and the uncertainty of the reference soundings was slightly larger in the Belize site. However, the lower uncertainty for the Belize site is attributable to the following factors: 1) the Landsat images covering the Belize site were generally cleaner (i.e., contained less image noise) and 2) the linear relationships between algorithm output and chart depths were stronger for the Belize site and less affected by the random perturbations to the inputs applied in the MC algorithm.

## Conclusions

This study indicates that a satellite-derived bathymetry procedure based on the Stumpf et al. (2003) algorithm can be used by national hydrographic offices to assess the adequacy of bathymetry on existing nautical charts. When deriving shallow-water bathymetry, it is important to consider the environmental conditions (e.g., water clarity, cloud cover, and sun glint) that could degrade the estimated accuracy for depths. In a practical sense, the procedure is best used as a reconnaissance tool for investigating coastal areas before a high-resolution hydrographic survey (e.g., MBES or ALB) is conducted. The two main data sources used in the procedure are the satellite imagery and a nautical chart. There is no need for tidal corrections or tide-coordinated imagery since reference soundings are used to adjust the algorithm output to physically meaningful depths, and simultaneously reference them to the chart datum.

The main limiting factor affecting the performance of satellite-derived bathymetry is the environment. Water clarity is a key factor that determines the penetration of light in water. The depth of the seafloor can only be estimated to the extent of this penetration. In particular, this process has limited application in turbid waters compared to clear waters. Other environmental factors include the presence of cloud cover in satellite images, atmospheric transmittance, sun glint, and substrate type. Cloud cover is often prevalent in tropical areas, and an effort needs to be made to select only images with less than 10% cloud cover without sun glint. Another challenge is the selection of reliable reference soundings that may be questionable due to the age of the hydrographic survey or the outdated technique and equipment used to conduct the survey. In such situations, it is recommended that the reference soundings be selected from those areas where the seafloor morphology shown on the chart and that derived from algorithm results are similar.

Preliminary results of the satellite-derived bathymetry indicate a good correlation between the algorithm results and the water depths. The procedure was verified in a U.S.

calibration study site (Rockport, MA) that contains a bathymetric reference dataset from an ALB survey and tidal information. Although the satellite-derived bathymetry was able to indicate the shallow-water bathymetry, it underestimated depth values in deeper areas. This error is due to the water clarity and can be reduced by selecting a satellite image that is collected at the flood stage of the tide when the suspended particulates in deeper areas are at a minimum within the tidal cycle. However, it is difficult to identify water clarity issues in areas close to the shoreline where turbidity is caused by wave and current action.

Finally, despite advances in satellite-derived bathymetry, the procedures described should be considered a reconnaissance tool for conducting hydrographic surveys. They are not a replacement for an acoustic (e.g., interferometric sonar or multibeam echosounders) or active remote sensing (e.g., ALB) hydrographic survey.



## Acknowledgements

The authors would to thank the anonymous reviewers for their comments that have improved the manuscript. Also, the authors want to thank NOAA and the UKHO for the copyright permission to use their charts for this study.

## Funding

This project was partially funded from the UNH / NOAA Joint Hydrographic Center grant NA05NOS4001153.

## References

Azuike, C., S. Pe'eri, A. Alexander, A. Armstrong, and C. Parrish. 2012. Development of a geospatial analysis methodology for assessing the adequacy of hydrographic surveying and nautical charting. Proceedings in the Canada Hydrographic Conference 2012, Niagara Falls, Canada, 15–17 May.

Bachmann, C., M. Montes, C. Parrish, R. Fusina, R. Nichols, R. Li, E. Hallenborg, C. Jones, K. Lee, J. Sellars, S. White, and J. Fry. 2012. A dual-spectrometer approach to reflectance measurements under sub-optimal sky conditions. *Optics Express* 20:8959–8973.

Barnhardt, W. A., B. D., Andrews1, S. D. Ackerman, W. E. Baldwin, and C. J. Hein 2007. High-Resolution Geologic Mapping of the Inner Continental Shelf: Cape Ann to Salisbury Beach, Massachusetts. USGS Open File Report 2007–1373.

Bramante, J. F., D. K Raju, and T. M Sin 2013. Multispectral derivation of bathymetry in Singapore's shallow, turbid waters, *International Journal of Remote Sensing* 34(6):2070–2088.

Dierssen, H. M., R. C. Zimmerman, R. A. Leathers, T. V. Downes, and C. O. Davis. 2003. Ocean color remote sensing of seagrass and bathymetry in the Bahamas Banks by high-resolution airborne imagery. *Limnology and Oceanography Methods* 48:444–455.

Flener, C., E. Lotsari, P. Alho, and J. Kayhko 2012. Comparison of empirical and theoretical remote sensing based bathymetry models in river environments. *River Research and Applications* 28:118–133.

Hedley, J. D., A. R. Harborne, and P. J. Mumby, 2005. Technical note: Simple and robust removal of sun glint for mapping shallow-water benthos. *International Journal of Remote Sensing* 26(10):2107–2112.

Hogfe, K. R., D. J. Wright, and E. J Hochberg 2008. Derivation and integration of shallow-water bathymetry: implications for coastal terrain modeling and subsequent analyses. *Marine Geodesy* 31:299–317.

International Hydrographic Organization (IHO). 2004. Publication C-55, Status of Hydrographic Surveying and Nautical Charting Worldwide, 3rd edition. Monaco: Author.

International Hydrographic Organization (IHO). 2008. IHO standards for hydrographic survey: Special Publication No. 44, 5th edition. Monaco: Author.

Jensen, J. R. 2007. Remote Sensing of the Environment: An Earth Resource Perspective, 2nd edition. Upper Saddle River, NJ: Prentice Hall Prentice Hall.

Jerlov, N. G. 1976. Marine Optics. New York: Elsevier Scientific.

Joint Committee for Guides in Metrology (JCGM). 2008a. Evaluation of measurement data – guide to the expression of uncertainty in measurement, Tech. Report, JCGM 100:2008, International Organization for Standardizationhttp://www.bipm.org/utils/common/documents/jcgm/JCGM_100_2008_E.pdf. Last accessed 22 May 2014.

—— 2008b. Evaluation of Measurement Data - Supplement 1 to the "Guide to the Expression of Uncertainty in Measurement - Propagation of Distributions Using a Monte Carlo Method. Tech. Report JCGM 101:2008. International Organization for Standardization. http://www.bipm.org/utils/common/documents/jcgm/JCGM_101_2008_E.pdf. Last accessed 22 May 2014.

Louchard, E. M, R. P. Reid, F. C. Stephens, C. O. Davis, R. A. Leathers, and T. V. Downeset. 2003. Optical remote sensing of benthic habitats and bathymetry in coastal environments at Lee Stocking Island, Bahamas: A comparative spectral classification approach. *Limnology and Oceanography: Methods* 48:511–521.

Lyzenga, D. R. 1978. Passive remote sensing techniques for mapping water depth and bottom features. *Applied Optics* 17:379–383.

Lyzenga, D. R. 1985. Shallow-water bathymetry using combined LiDAR and passive multispectral scanner data. *International Journal of Remote Sensing* 6: 115–125.

Lyzenga, D. R., N. P. Malinas, and F. J. Tanis. 2006. Multispectral bathymetry using a simple physically based algorithm. *IEEE Transactions on Geoscience and Remote Sensing* 44:2251–2259.

Maritorena, S., A. Morel, and B. Gentili. 1994. Diffuse reflectance of oceanic shallow waters: Influence of water depth and bottom albedo. *Limnology and Oceanography: Methods* 39:1689–1703.

Mikhail, E. 1976. Observations and Least Squares. Lanham, MD: University Press of America.

Mobley, C. D. 2004. Light and Water: Radiative Transfer in Neutral Waters [CD Rom]. San Diego, CA: Academic Press.

Mobley, C. D., H. Zhang, and K. J. Voss. 2003. Effects of optically shallow bottom on upwelling radiances: Bi-directional reflectance distribution function effects. *Limnology and Oceanography: Methods* 48:337–345.

Myers, E., K. Hess, Z. Yang, J. Xu, A. Wong, D. Doyle, J. Woolard, S. White, B. Le, S. Gill, and G. Hovis. 2007. VDatum and strategies for national coverage. Proceedings of the Marine Technology Society/IEEE OCEANS Conference, Vancouver, British Columbia, Canada.

National Oceanic and Atmospheric Administration (NOAA). 2009a. Chart 13279: Ipswich Bay to Gloucester Harbor, 33rd edition. Scale: 1:20,000. Silver Spring, MD.

National Oceanic and Atmospheric Administration (NOAA). 2009b. Chart 13278: Portsmouth to Cape Ann, 27th edition. Scale: 1:80,000. Silver Spring, MD.

National Oceanic and Atmospheric Administration (NOAA). 2012. Vertical Datum Transformation: VDatum 3.1. http://vdatum.noaa.gov/. Last accessed December 2012.

Papadopoulos, C.E., and H. Yeung. 2001. Uncertainty estimation and Monte Carlo simulation method. *Flow Measurement and Instrumentation* 12(4): 291–298.

Pe'eri, S., J. V. Gardner, L. G. Ward, and J. R. Morrison. 1996. The seafloor: A key factor in LiDAR bottom detection. *IEEE Transactions on Geoscience and Remote Sensing* 5: 1266–1271.

Philpot, W. D. 1989. Bathymetric mapping with passive, multispectral imagery. *Applied Optics* 28:1569–1578.

Philpot, W. D., C. O. Davis, W. P. Bissett, C. D. Mobley, D. D. R. Kohler, Z. Lee, J. Bowles, R. G. Steward, Y. Agrawal, J. Trowbridge, R. W. Gould, Jr., and R. A. Arnone. 2004. Bottom characterization from hyperspectral image data. *Oceanography* 17(2):76–85. http://dx.doi.org/10.5670/oceanog.2004.50.

Powell, J., C. Ence, T. Wallace, A. Jett, K. O'Dell, M. Lewis, J. Arias, and T. Kearns. 2009. Using ArcGIS Nautical Solution to Produce Navigational Products. Proceedings of the U.S. Hydrographic Conference, Norfolk, VA.

Robinson, I. S. 2004. Measuring the Oceans from Space: The Principles and Methods of Satellite Oceanography. Chichester: Praxis Publishing.

Sandidge, J.C., and R.J. Holyer 1998. Coastal bathymetry from hyperspectral observations of water radiance. *Remote Sensing Environment* 65:341–352.

Stumpf, R. P., K. Holderied, and M. Sinclair. 2003. Determination of water depth with high-resolution satellite imagery over variable bottom types. *Limnology and Oceanography: Methods* 48:547–556.

Su, H., H. Liu, and W. D. Heyman. 2008. Automated derivation of bathymetric information from multi-spectral satellite imagery using a non-linear inversion model. *Marine Geodesy* 31:81–298.

Vanderstraete, T., R. Goossens, and T. K. Ghabour. 2006. The use of multi-temporal Landsat images for the change detection of the coastal zone near Hurghada, Egypt. *International Journal of Remote Sensing* 27(17):3645–3655.

Vogelmann, J. E., D. Helder, R. Morfitt, M. J. Choate, J. W., Merchant, and H. Bulley. 2001. Effects of Landsat 5 thematic mapper and Landsat 7 enhanced thematic mapper plus radiometric and geometric calibrations and corrections on landscape characterization. *Remote Sensing Environment* 78:55–70.

U.S. Geological Survey (USGS). 2006. Landsat 7 (L7) Image Assessment System (IAS) Geometrical Algorithm Theoretical Basis Document (ATBD), Tech. Report LS-IAS-01.

United Kingdom Hydrographic Office (UKHO). 1989. Admiralty Chart 1797: Monkey River to Colson Point (latest edition 24 December 2009). Scale: 1:125,000. Taunton, UK.

United Kingdom Hydrographic Office (UKHO). 2000. Admiralty Chart 3321: Entrances to Escravos and Forcados Rivers (latest edition 31 July 2008). Scale: 1:60,000. Taunton, UK.